# Magnetic domains and domain-wall structure in Ni/Cu(001) films imaged by spin-polarized low-energy electron microscopy

R. Ramchal,[1] A. K. Schmid,[2] M. Farle,[1] and H. Poppa[2]
[1]*Institut für Physik, Universität Duisburg-Essen, Lotharstrasse 1, 47048 Duisburg, Germany*
[2]*NCEM, Lawrence Berkeley National Laboratory, Berkeley, California 94720, USA*
(Received 21 October 2002; revised manuscript received 28 May 2003; published 25 August 2003)

The magnetic domain microstructure of four- to eight-monolayer- (ML-) thick Ni/Cu(001) films deposited at 100 K and 300 K was studied at both temperatures by spin-polarized low-energy electron microscopy. Domain structures remain stable during deposition: large in-plane domains of several 10 $\mu$m diameter persist at both temperatures throughout the thickness range. The position of the domain walls is not significantly correlated with topographic features (step bunches, terraces) which were imaged simultaneously. The structure of 180° Néel walls in the films was determined by using the spin manipulator of the electron illumination system to measure image contrast as a function of polar and azimuthal polarization of the illuminating beam. We find that in 8-ML films at 300 K, the Néel walls are 400 nm wide and wall segments with both expected chiralities were identified.

DOI: 10.1103/PhysRevB.68.054418 PACS number(s): 75.70.Ak, 75.70.Kw, 68.37.Nq, 68.55.Jk

We address the question of how magnetic domain microstructure in a quasi-two-dimensional ferromagnet might depend on layer thickness and temperature. In the thickness range of a few monolayers, epitaxial fct Ni films grown on Cu(001) single crystals are one prototypical example of such systems. From previous studies by many groups, macroscopic magnetic properties such as Curie temperature, magnetic anisotropy, and magnetic moments as a function of film thickness are well described.[1–3] However, relatively few studies have addressed the system's magnetic microstructure. Domain structures in up to 14-nm-thick Ni/Cu/Si(001) films capped with 2 nm Cu (Refs. 4 and 5) and in up to 220-nm-thick films (Ref. 6) have been observed by magnetic force microscopy (MFM) and by the magneto-optic Kerr effect (MOKE).[7,8] Interestingly, no *in situ* magnetic domain observations have been reported for uncapped Ni/Cu(001) films thinner than eight monolayers (ML) where the Ni layers are in-plane magnetized. In this thickness regime the presence of step bunching and roughness at the substrate may play an important role for the pinning and direction of magnetic domain walls. One of the best techniques to study the correlation of topography and magnetic domain walls is spin-polarized low-energy electron microscopy (SPLEEM). In the present work, this technique (SPLEEM) is used to investigate the magnetic domain structure of in-plane magnetized uncoated Ni/Cu(001) film prepared *in situ*. Characteristic differences to out-of-plane magnetized Fe/Cu(001) (Refs. 9 and 10) and Co/Cu/Co (Ref. 11) which have been previously studied by SPLEEM are expected and observed.

Magnetic domains in 4–8 ML Ni on Cu(001) were imaged by spin-polarized low-energy electrons at 300 K and 100 K. SPLEEM is a surface sensitive method with a lateral resolution of 10 nm and a relatively high image acquisition rate of about 5 frames per second. SPLEEM images were recorded before, during and after *in situ* film growth. Exploiting the method's sensitivity to topographic features such as atomic surface steps and step bunches and its capability to simultaneously record magnetic contrast images, we were able to directly correlate topography and magnetic domain formation during deposition.

We used a carefully developed substrate cleaning procedure, which we had found to be effective to suppress possible bunching of atomic steps. Suppression of step bunching in substrate surfaces is an important issue in magnetic microstructure research, because even in otherwise highly perfect epitaxial ultrathin films, substrate step bunches can easily act as pinning sites for magnetic domain walls and thus influence the samples' magnetic properties. Before each experiment, our Cu crystal was prepared by 12 h of Ar-ion sputtering using a low current of approximately 0.1 $\mu$A/cm$^2$ and ion energy in the range of 1.5–3 kV. During sputtering, the crystal was automatically flash annealed to approximately 1000 K in 10-min intervals. After this preparation schedule, no surface contamination was detectable using our single-pass cylindrical mirror Auger electron spectrometer. Imaging the bare Cu(001) substrate in the SPLEEM, we confirmed that the resulting surface had atomically flat terraces separated by mostly monoatomic steps. Ni films were deposited *in situ*, with the Cu(001) substrate held at either 100 K or 300 K. The evaporator target was a high purity rod of 2 mm diameter, which was brought to sublimation temperature by direct electron beam heating inside a water-cooled doser. The base pressure during imaging was $2\times10^{-8}$ Pa; the maximum pressure during evaporations reached $4\times10^{-8}$ Pa.

In the SPLEEM, a spin-polarized low-energy electron beam is directed at the sample surface at normal incidence, and the specular beam is magnified in an electron-optical column to form a real-space image of the sample or a back-scattered electron diffraction pattern. This image can be recorded in real time at up to video rate. As described in Ref. 10, the SPLEEM can be used for convenient and very precise film-thickness control during *in situ* film growth by monitoring the average intensity of the image beam. The periodic nucleation, growth, and completion of atomic monolayers during epitaxial growth leads to well-known diffraction intensity oscillations.[12] A typical example of a film grown at

 

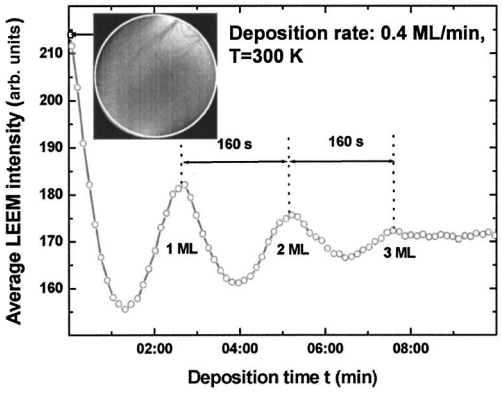


FIG. 1. Film thickness calibration by the oscillation of the integrated LEEM intensity during Ni deposition at 300 K. The maxima indicate full atomic Ni layers, and their distance in time determines the deposition rate to equal 0.4 ML/min. Each point corresponds to a LEEM image. The inset shows the topography of the atomically flat Cu(001) substrate before deposition (field-of-view diameter 10 $\mu$m). The LEEM intensity is integrated over the area given by the circle.

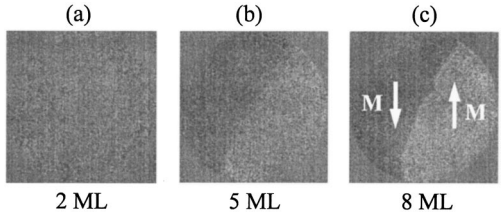


FIG. 2. Appearance of in-plane magnetic contrast at room temperature: (a) 2 ML, (b) 5 ML, and (c) 8 ML Ni/Cu(001). The diameter of the field of view is 10 $\mu$m.

300 K is shown in Fig. 1, where the average intensity of the image beam is plotted as a function of time. The distance between two maxima yields the deposition rate, i.e. typically 0.4 ML per minute in our experiments. We attribute the reduced amplitude of each following maximum (minimum) to roughness effects that increase with increasing number of atomic layers. Films grown at 100 K show a reduced amplitude and a faster decay of the oscillations indicating a higher degree of roughness.

While simultaneously monitoring film growth, we used the SPLEEM to observe the evolution of magnetic domain microstructures. Before discussing our results on the magnetism of Ni/Cu(001), we briefly describe how magnetic contrast originates in this microscope. The magnetic contrast in SPLEEM images (MC) is related to the relative orientations of the magnetization **M** in the film and the beam polarization **P** according to $\mathrm{MC} \propto \mathbf{P} \cdot \mathbf{M}$. Being based upon spin-dependent exchange scattering of the spin-polarized illuminating beam, the magnetic image contrast in reflected intensities for electrons with their polarizations parallel and antiparallel with respect to the local sample magnetization is typically of the order of 1%. To enhance the contrast, we toggle the illumination polarization by 180° from image to image, so that a differential imaging method can be employed.[13] The method is based on the usual definition of exchange asymmetry $A_{\mathrm{ex}} = 1/|\mathbf{P}|(I_+ - I_-)/(I_+ + I_-)$ where $I_+$ and $I_-$ represent the reflected intensities for oppositely polarized incident beams. Subtraction of $I_+$ (spin-up) and $I_-$ (spin-down) images in the numerator eliminates nonmagnetic diffraction and topographical image features. Only features which originate exclusively in the magnetism of the sample are left in the image.

The necessary capability to quickly toggle the polarization of the illumination beam is a general feature of the Pierce-type[14] GaAs-based photoemission source we used, where the polarization of the emitted electron beam can be switched from spin up to spin down simply by switching the photon polarization from left-hand to right-hand helicity. In addition, in the instrument used here, the electron beam passes through a spin manipulator prior to illuminating the sample. This spin manipulator features two magnetic rotator lenses in combination with an electrostatic 90° deflector. Controlled excitation of these three elements permits independent rotation of the beam polarization in both the polar and azimuthal angular orientations. Imaging with various beam polarizations allows a complete characterization of the local magnetization vector in the sample surface. For details about the instrument see Refs. 15–18.

Spin-dependent magnetic contrast is determined by the spin-dependent band structure. Consequently, the exchange asymmetry[19] oscillates with energy. To find the optimum contrast for our samples we took several series of SPLEEM images at different electron energies and different Ni film thicknesses. The exchange asymmetry oscillates between 4 and 11 eV with a maximum at about 9.2 eV. Note that from these experimental values the difference of the work functions of sample and cathode has to be subtracted (about 3 eV). At about 4.5 eV the MC is reversed and much weaker than at 9.2 eV. Between 5 and 8 ML the maximum shifted only by a few tenths of eV. All images presented in this paper were recorded at $E = 9.5$ eV.

Consistent with earlier determinations of the thickness-dependent Curie temperature[20] *in situ* SPLEEM observation during room-temperature growth shows no magnetic contrast in the thickness range below 5 ML. When the thickness of the growing film increases beyond 5 ML, we observe an abrupt onset of magnetic contrast with the magnetization vector lying in-plane. An example is shown in Fig. 2, where the spontaneous formation of two in-plane domains with anti-aligned magnetizations **M** (indicated by the white arrows) has resulted in a domain wall crossing the field of view near the center. Interestingly, no percolation of smaller magnetic domains at the onset of ferromagnetism was observable, when the film thickness was increased in 0.1-ML steps across the threshold (about 4.8 ML) for ferromagnetism at 300 K. The position and structure of this domain wall remain unchanged during subsequent deposition of additional Ni up to a thickness of 8 ML. For a film grown at 100 K the onset to ferromagnetism was observed at lower thickness in agreement with the well-established magnetic phase diagram[2,3] of Ni/Cu(001). Aside from this lower onset of magnetic contrast no characteristic changes of domain sizes and shapes were

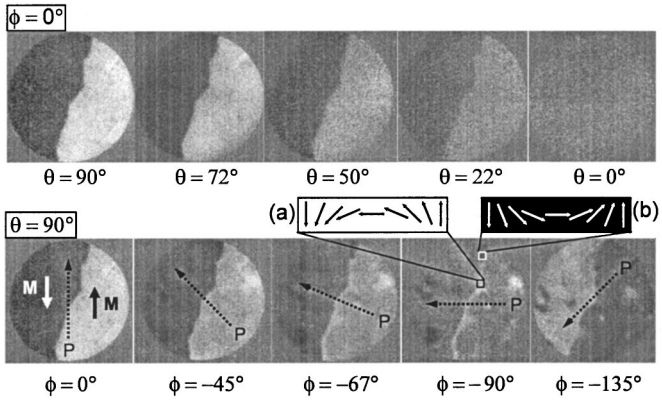


FIG. 3. SPLEEM images of an 8-ML Ni/Cu(001) film at 300 K as a function of the polar angle $\theta$ (top, $\phi=0°$) and azimuthal angle $\phi$ (bottom, $\theta=90°$) of the polarization **P** of the electron beam with respect to the sample normal. Top: sharp magnetic contrast with the polar angle in the film plane (left), no contrast with $\theta$ perpendicular to the surface (right): i.e., the Ni film is fully in-plane magnetized. Bottom: at $\phi=0°$ the MC is maximum: the domains are parallel and antiparallel with respect to the polarization direction. The magnetic contrast disappears at $\phi=-90°$. Two chiralities exist in the Néel wall, as seen in the image ($\phi=-90°$). Due to (a) parallel and (b) antiparallel orientations, the Néel wall appears white and black, respectively.

observed between 100 K and 300 K growth when the field of view (10 $\mu$m diameter) was manually scanned over a 2 $\times 2$ mm$^2$ area.

The structure of the domain wall in the 8-ML Ni/Cu(001) film seen in Fig. 2 was analyzed in greater detail, as shown in Fig. 3. First, while keeping the azimuthal angle fixed at $\phi=0°$, the polar angle $\theta$ of the electron beam polarization was varied in steps from $\theta=90°$ (spin polarization in-plane) to $\theta=0°$ (spin polarization along the surface normal). Diminishing contrast in this series confirms the absence of out-of-plane magnetization components: i.e., the local magnetization vector lies in the surface plane in both domains. Then, the polar alignment of the illumination beam polarization was fixed at $\theta=90°$ (spin polarization in-plane) and the azimuthal polarization orientation was swept through an angle of $-135°$. The magnetic contrast between the domains can be seen to decrease in this series: it finally vanishes when the beam polarization is perpendicular to the magnetization vectors of the two domains. The absence of magnetic contrast between the two domains for the alignment $\phi=-90°$ confirms that the two domains are anti-aligned and are thus separated by a 180° domain wall. In all but the $\phi=0°$, additional contrast can be discerned in the region of the domain wall. Most clearly at $\phi=-90°$, a large section of the domain wall appears brighter and a shorter segment near the top of the image appears dark. Our interpretation of this contrast is that the domain wall has a Néel structure, in which the spin reorientation between the two anti-aligned domains takes place within the film plane. The fact that different sections of the wall show opposite contrast is consistent with the expectation that Néel walls must occur in two degenerate chiralities, as indicated schematically in the figure.

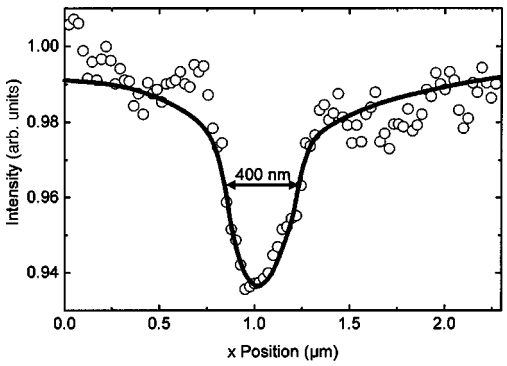


FIG. 4. The profile plot of the white imaged Néel wall with the electron polarization at $\theta=90°$, $\phi=-90°$ (Fig. 3, bottom) reveals an average wall width of 400 nm. The solid line is a guide to the eye according to the calculated profiles of a symmetric 180° Néel wall (Refs. 21 and 22).

To confirm this interpretation we show in Fig. 4 the averaged line profile across the 180° domain wall of the SPLEEM image ($\phi=-90°$), shown in Fig. 3 (lower panel). The profile consisting of the average of about 50 parallel profile lines shows the typical shape of a Néel wall consisting of a narrow core and a long tail as discussed in Ref. 22, p. 244. The solid line in Fig. 4 is a guide to the eye according to the calculation in Ref. 22. The core width is determined to be about 400 nm (Fig. 4). We find good agreement with calculated profiles of Néel walls[21] for which the width can be estimated by $\delta=\pi\sqrt{2A/K_{\text{eff}}}$ (Ref. 24) using the exchange constant $A=0.75\times10^{-11}$ J/m, which is the average of values given for Ni thin films with 157–250 nm thickness,[26] and an effective magnetic anisotropy parameter $K_{\text{eff}}=K_2+K_{\text{shape}}=0.9\times10^3$ J/m$^3$. The parameter $K_{\text{eff}}$ which includes shape ($K_{\text{shape}}$) and second-order magnetocrystalline anisotropy ($K_2$) is about one order of magnitude smaller than the experimentally determined $K_{\text{eff}}$ of a 8-ML Ni film on Cu(001) at room temperature.[3,20] Such a difference by orders of magnitude was also observed for Co monolayers on Cu(100) (Ref. 23) where a Néel wall width of about 500 and 300 nm was measured for 5.5 and 9 ML. One should note here that a calculation for the Néel walls of ''negative anisotropy materials'' favoring $\langle 111\rangle$ directions like Ni should be corrected by taking magnetostriction effects into account, yielding a wall width $\delta=6.5$ through $7.2\sqrt{A/K_{\text{eff}}}$ (p. 234 of Ref. 22) in better agreement to our experimental observation. In difference to the expected decrease of the Néel-wall width for thicker films the domain wall width in Ni/Cu(001) increases from about 330 nm at 5 ML to 450 nm at 9 ML and dramatically broadens to 1400 nm (yielding a very small $K_{\text{eff}}<10^2$ J/m$^3$) at the start of the spin-reorientation transition (SRT) (Ref. 20) near 9.5 ML. This enormous increase of the domain-wall width within a few tens of monolayers can be explained by the decrease of the effective magnetic anisotropy (proportional to the reciprocal thickness). Eventually $K_{\text{eff}}\rightarrow 0$ disappears at the SRT as the result of the compensation of the in-plane shape anisotropy and out-of-plane, spin-orbit-induced (magnetocrystalline) anisotropy.[2,3] To quantitatively check the theoretical predicted shape and width of

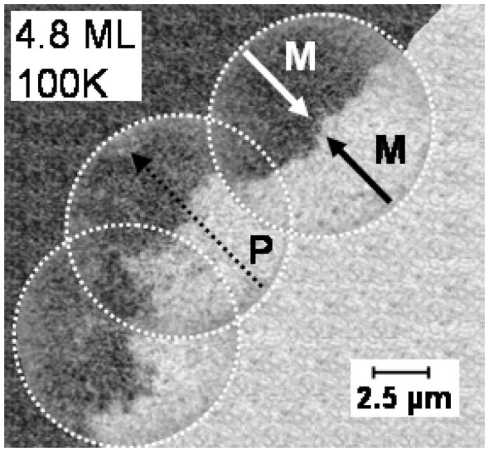


FIG. 5. Three SPLEEM images with 10-$\mu$m field of view (circles) tracing a domain wall of a 4.8-ML-thick Ni film prepared at 300 K and measured at 100 K. The domain sizes are several 10 $\mu$m. No preferred direction of the domain wall with respect to crystallographic axes was found.

domain walls in magnetic monolayers one needs accurate knowledge of the magnetic anisotropy $K_{\mathrm{eff}}$ and the exchange constant $A$ which turns out to be not available in many systems. For example, to obtain a quantitative agreement between the experimentally measured wall width of in-plane magnetized 1 ML Fe/W(110) (Ref. 27) and the calculated one according to $\delta \propto \sqrt{A/K_{\mathrm{eff}}}$, the exchange constant $A$ had to be assumed one order of magnitude smaller than the bulk value and $K_{\mathrm{eff}}$ turned out to be more than two orders of magnitude larger than typical Fe film values.

In Fig. 5 we show the MC images of a 4.8-ML Ni/Cu(001) film prepared at 300 K and measured *in situ* at 100 K. For maximum contrast we rotated the polarization **P** of the electron beam in the film plane. For **P** perpendicular to the film surface no MC was observed, confirming the in-plane orientation of **M**. Our microscopic observation of in-plane magnetization is again in good agreement with Ref. 20. Again, we observed large domains with sizes of several 10 $\mu$m, substantially larger than our 10-$\mu$m maximum field of view. To confirm that our SPLEEM images of these domain walls are representative of typical configurations, we traced domain walls over extended distances. In the example of Fig. 5 the imaged area (circles) was moved in several steps to trace the domain wall. The correct alignment of the magnetic images was unambiguously verified by comparing surface-step patterns in the corresponding LEEM images, which are not shown here. Close inspection of the ''spin-up'' and ''spin-down'' LEEM topographic images and comparison with the corresponding magnetic images reveals no correlation between the topography of the Ni film and its magnetic domain structure. For example, we did not find evidence for domain-wall pinning at atomic step bands. Comparing the images of Figs. 2(c), 3, and 5 one observes a difference in the smoothness of the domain walls but no change in domain sizes. The increased wall roughness of the film measured at 100 K (Fig. 5) can be attributed to two effects: (a) when cooling from 300 K to 100 K in $1.5\times10^{-8}$ Pa trace amounts of residual gases (CO, $CO_2$) may adsorb, which reduce the total magnetic anisotropy in the 5-ML regime considerably, and (b) the formation of a zigzag domain wall which is not completely resolved. Such domain walls are known[22] to originate from ''head-on'' 180° domain walls. One should note, however, that we find no statistically significant differences between the domain structures at 100 K and 300 K for up to 8 ML thickness when comparing many images recorded in different areas of films grown at 100 K and 300 K. Our SPLEEM apparatus does not provide the high resolution ($<5$ nm) to resolve fine details of the domain-wall structure as, for example, spin-polarized scanning tunneling microscopy (SP-STM) techniques do (see, for example Ref. 25). On the other hand, SP-STM or secondary electron microscopy with polarization analysis techniques do not allow a fast magnetic contrast acquisition over the large areas imaged here.

Above 8 ML we find evidence for a continuous rotation of large areas of the magnetization from in-plane to out-of-plane originating at the domain walls. No breakup into a stripe or meandering domain pattern is observed. A detailed discussion is beyond the scope of this paper and will be published elsewhere.

In summary, the domain structure of uncapped ultrathin Ni/Cu(001) films in the thickness range of 4.8–8 ML, prepared and measured at 100 K and 300 K, was observed by spin-polarized low-energy electron microscopy. This technique allows visualization of magnetic domains with high spatial as well as time resolution and good angular resolution of the local orientation of the magnetization vector. Large domains of several 10 $\mu$m width were found in the virgin state at 100 K and 300 K. Using the case of a 180° Néel wall in an 8-ML Ni/Cu(001) film as an example, we have shown how the detailed structure of domain walls can be resolved through polarization-dependent measurements.

R.R. thanks the Deutscher Akademischer Austauschdienst for financial assistance. This work was supported by the U.S. Department of Energy, Contract No. DE-AC3-76SF00098 and Deutsche Forschungsgemeinschaft.

[1] R. Vollmer, Th. Gutjahr-Löser, J. Kirschner, S. van Dijken, and B. Poelsema, Phys. Rev. B **60**, 6277 (1999).
[2] K. Baberschke, Appl. Phys. A: Mater. Sci. Process. **62**, 417 (1996); P. Poulopoulos and K. Baberschke, J. Phys.: Condens. Matter **11**, 9495 (1999).
[3] M. Farle, Rep. Prog. Phys. **61**, 755 (1999).
[4] H. J. Hug *et al.*, J. Appl. Phys. **79**, 5609 (1996).
[5] G. Bochi *et al.*, Phys. Rev. Lett. **75**, 1839 (1995).
[6] S. Hameed *et al.*, Phys. Rev. B **64**, 184406 (2001).
[7] A. Bauer, E. Mentz and G. Kaindl, J. Magn. Magn. Mater. **198–199**, 489 (1999).
[8] S. P. Li *et al.*, Phys. Rev. Lett. **88**, 087202 (2002).

[9] K. L. Man, M. S. Altman, and H. Poppa, Surf. Sci. **480**, 163 (2001).
[10] K. L. Man *et al.*, Phys. Rev. B **65**, 024409 (2001).
[11] T. Duden and E. Bauer, J. Magn. Magn. Mater. **191**, 301 (1999).
[12] C. M. Schneider, A. K. Schmid, P. Schuster, H. P. Oepen, and J. Kirschner, in *Magnetism and Structure in Systems of Reduced Dimension*, edited by R. F. C. Farrow *et al.* (Plenum Press, New York, 1993), pp. 453–466.
[13] M. S. Altman *et al.*, in *Magnetic Materials: Microstructure and Properties*, edited by T. Saonki *et al.*, Mater. Res. Soc. Symp. Proc. No. **232** (Material Research Society, Pittsburgh, 1991), p. 125.
[14] D. T. Pierce *et al.*, Rev. Sci. Instrum. **51**, 478 (1978).
[15] K. Grzelakowski, T. Duden, E. Bauer, H. Poppa, and S. Chiang, IEEE Trans. Magn. **30**, 4500 (1994).
[16] K. Grzelakowski and E. Bauer, Rev. Sci. Instrum. **67**, 742 (1996).
[17] T. Duden and E. Bauer, J. Electron Microsc. **47**, 379 (1998).
[18] E. D. Tober, G. Witte, and H. Poppa, J. Vac. Sci. Technol. A **18**, 1845 (2000).
[19] E. Bauer, T. Duden, H. Pinkvos, H. Poppa, and K. Wurm, J. Magn. Magn. Mater. **156**, 1 (1996).
[20] K. Baberschke and M. Farle, J. Appl. Phys. **81**, 5038 (1997).
[21] A. Holz and A. Hubert, Z. Angew. Phys. **26**, 145 (1969).
[22] A. Hubert and R. Schäfer, *Magnetic Domains* (Springer, Berlin, 1998).
[23] A. Berger and H. P. Oepen, Phys. Rev. B **45**, 12 596 (1992).
[24] R. C. O'Handley, *Modern Magnetic Materials: Principles and Application* (Wiley, New York, 2000).
[25] Haiqiang Yang, A. R. Smith, M. Prikhodo, and W. R. L. Lambrecht, Phys. Rev. Lett. **89**, 226101 (2002) and references therein.
[26] H. P. J. Wijn, in *Condensed Matter*, edited by H. P. J. Wijn, Landolt-Börnstein, New Series, Group III, Vol. 19, Pt. G (Springer-Verlag, Berlin, 1988), p. 101.
[27] M. Pratzer *et al.*, Phys. Rev. Lett. **87**, 127201 (2001).